IET Smart Grid

Special issue Call for Papers

Be Seen. Be Cited.
Submit your work to a new IET special issue

"Deep learning assisted Energy Efficiency Strategies for Sustainable Smart Grids"

Guest Editors: Iskander Tlili, Ahmed Awan, Sa'ed Awni Musmar, Vishwanath Deshmane and Mahendran Samykano

Read more

50% APC Discount code IET50 on submission.

The Institution of Engineering and Technology

Received: 9 October 2020 | Revised: 26 December 2020 | Accepted: 17 January 2021

IET Smart Grid

DOI: 10.1049/stg2.12018

The Institution of Engineering and Technology WILEY

ORIGINAL RESEARCH PAPER

Analysis of current density in the electrode and electrolyte of lithium-ion cells for ageing estimation applications

Mehrnaz Javadipour | **Kamyar Mehran**

School of Electronic Engineering and Computer Science, Queen Mary University of London, Mile End Road, London, E1 4NS, UK

Correspondence

Kamyar Mehran, School of Electronic Engineering and Computer Science, Queen Mary University of London, Mile End Road, London, UK, E1 4NS
Email: k.mehran@qmul.ac.uk

Abstract

Lithium-ion battery is the commonly used energy storage technology in electric vehicles (EVs) because of its inexpensive manufacturing cost and high energy capacity. For optimal utilization of its capacity and lifetime, reliable state of health (SoH) monitoring solutions have to be included in the battery management system (BMS). SoH of a cell is affected by several reasons such as internal degradation or external damages that need to be estimated. This article analyses the current density in electrode and electrolyte of an EV lithium-ion cell using a simulation assisted method that leads to improvement in SoH estimation accuracy. The experimental results are analysed through the fusion of the magnetic field images captured by quantum fluxgate magnetometers, installed on the surface of the cell, together with the real-time simulation of the multi-physics model of the cell. The magnetic field sensors measure the magnetic field intensity with an accuracy of ±2 mT. The real-time simulation input data is updated from the measurements of both the magnetic field sensors and the battery cycler. The multi-physics model of the cell is developed in COMSOL modelling software, and real-time data fusion process is implemented on dSPACE Microlabbox real-time simulator. Results confirm that the proposed monitoring solution provides useful insight that can be employed in ageing estimation of EV batteries.

1 | INTRODUCTION

Electric vehicles (EVs) and renewable energy sources (RES) are the two examples of modern technologies that are developed based on the advances in energy storage systems (ESSs) [1–3]. EVs use ESSs for their fully electric operation and RES benefit from ESSs as a temporary storage for power stabilization because of their intermittent power profile [4–6]. Therefore, the performance of the mentioned examples is directly affected by the operating condition of their ESSs.

Among all the energy storage technologies, lithium-ion batteries (LIBs) are the most commonly used ones because of their inexpensive manufacturing costs and easier maintenance in smaller size. LIBs, comparing to the other technologies, have longer life cycles, higher rate of charge/discharge, and high energy density, resulting in large capacity suitable for industrial use cases [7,8]. In contrast to their many advantages, LIBs require a reliable condition monitoring system to monitor their state of health (SoH) and state of charge (SoC) due to the safety and operational issues associated with them. The condition monitoring system is especially crucial for EVs as reliability is highly required, with low maintenance costs.

Condition monitoring of LIBs is usually summarized as SoC and SoH estimation in the literature [9]. Ageing is the main factor in SoH estimation. LIBs have a limited number of charging/discharging cycles that makes them unusable after a while [10]. A high number of research have been made to understand ageing in lithium-ion batteries [11–13]. Furthermore, mechanical degradation in LIBs is another factor that affects the SoH in a battery. The monitoring of SoC and SoH in LIBs has been studied in several works such as [14–16] to name a few. In [15], the measurement of small induced magnetic field changes in a cell have been studied to be used for assessment of the lithium incorporation level into the electrode materials and to detect certain defects in a cell. In [14], the role of negative electrode porosity in long-term ageing of LIBs has been analysed. It was shown that lithium can only participate to SEI (solid electrolyte interphase) growth, which decreases the capacity by lithium consumption.

Considering the challenges and drawbacks of the existing methods in SoH estimation [17,18], some improvements have been made to tackle the problems by proposing smarter SoC and SoH estimation systems with more accurate results to prevent possible hazards [19]. There are high chances of fire or explosion when the LIBs are used in high temperature environments or under short circuit faults [20]. It is mandatory to include a degree of operational awareness in the battery management systems (BMS) [21,22]. Therefore, a low-cost battery monitoring method is required to improve the utilization efficiency, and to maximize the safe operation lifetime.

The commonly used techniques for SoC estimation such as terminal voltage measurement and coulomb counting are not accurate enough to model the ageing in performance degradation of LIBs [14]. This is due to the nature of the LIBs, which internally expose different complex non-linear chemical processes [23,24]. Although the manufacturing cost of LIBs is decreasing every year, still high-capacity batteries are expensive and require a suitable monitoring system for longer operation. In [25], a fast non-destructive method of magnetic field monitoring is introduced for detecting defects such as capacity fade and mechanical degradation inside a cell. Beside analysing the defects, magnetic field around the lithium-ion cell has also provided useful information for temperature estimation in LIBs [26]. There are two main sources for the magnetic fields around the lithium-ion cell: (1) surface currents in the electrode, and (2) charge transfer currents in the electrolyte. The behaviour of these currents in a cell determines the magnetic field around a cell as is shown in [26], which provides significant insight of the cell operational state.

Internal current distributions modelling in the electrodes and electrolyte, even for a few numbers of cycles, is difficult due to the complex computations required for simulation. Several examples of representation for the internal behaviour of batteries can be found in literature, including terminal voltage, SoC, current density and temperature distribution. Nevertheless, measuring the distribution of the cell's internal current density using direct methods is a subject that can be found in only a few articles. Authors in [27] created a prototype cell in a lab-scale size, which was designed for analysing the distribution of current density inside of the electrode along its height and width. In this paper, the distribution of cell's current via the formation process of the graphite electrode has been investigated. Similarly, in [28], several aged electrodes were analysed to present that even small current densities can cause intense gradients inside the electrodes with its subsequent effect on the magnetic fields. In another example, authors in [29] created a particular LFP/Graphite prototype cell for this purpose. In this work, the cell's current distribution while discharging at varying temperatures and C-rates was analysed using a segmented cathode. This set-up allows for an accurate monitoring of each electrode's current, individually.

To address the aforementioned challenges in direct SoH estimation of LIBs, this paper has analysed the current density in electrode and electrolyte of an EV lithium-ion cell using a simulation assisted method in order to show how this information leads to a more accurate SoH estimation. Measurement of electrolyte and electrode current densities are achieved using magnetic field images from magnetometers, installed on the surface of the cell. With the help of COMSOL modelling software, a simulation assisted framework is developed to validate the contribution of magnetic field images to the SoH of the LIB. In this work, the lithium-ion cell for the case study has current collectors made of Aluminium and Copper, electrodes made of $Li(Ni_{1/3}Mn_{1/3}Co_{1/3})O_2$ (NMC) and Graphite, and electrolyte made of LiPF6 in 3:7 EC:EMC.

The rest of article is organised as follows. Section 2 provides a thorough comparison of the existing SoH estimation methods with the applications in smart grid. In Section 3, preliminaries of current density calculation in lithium-ion cells are provided. Then after, in Section 4, the experimental framework configuration for the analysis of the magnetic field images is discussed and it is shown how the current density graphs are captured. The experimental results are then discussed in detail in Section 5 in different test cases. It is shown that how current density can be used as a measure for SoH estimation of LIBs. Finally, results of the paper are concluded in Section 6.

2 | STATE OF THE ART, CHALLENGES, AND OUTLOOK

In this section, after discussing the challenges in SoH estimation, a thorough review of the most recent works in SoH estimation of LIBs is provided. Also the comparison of the mentioned methods is summarized in Table 1.

One of the main challenges in the design of BMS for LIBs is to consider the irreversibility in the degradation process [10]. Capacity fading is directly related to SoH, which is usually defined as the ratio of current energy capacity to the initial energy capacity. Different from SoC estimation methods, which rely on open-circuit voltage (OCV) measurement [30], there is no single well-known parameter, which reflects the health of the battery with high accuracy. Hence, SoH estimation becomes a multi-parameter problem by finding a health indicator (HI) expression, which can be readily acquired and computed. The SoH is then estimated by feeding the HI to the estimator established using experimental and simulation data.

A common source of HI for LIBs is the terminal voltage. Studies on battery ageing mechanisms revealed that the loss of active materials and lithium-ion inventory increase the internal impedance of the battery and affects the polarization voltage [31]. Electrochemical impedance spectroscopy (EIS) is a widely used frequency domain method to characterise the impedance and estimate the SoH [32]. Based on this method, authors in [33] proposed a novel non-destructive SoH estimation to identify charge transfer impedance and Ohmic impedance from internal impedance. The transformation of Warburg diffusion impedance from frequency domain to time domain can also be realised using this method. On top of that, authors in [34] have found three specific resonance frequencies at which impedance shows highest relation to the health of the battery. Nevertheless, EIS-based methods are expensive, time

TABLE 1 Comparison of the most common SoH estimation methods in terms of accuracy, computational complexity, on-board operations, and time consumption

SoH estimation method	Accuracy	Computational complexity	Operating on-board	Time consumption
Measuring the internal resistance [30,31]	High	Low	Not supporting	High
Measuring the internal impedance [32,33]	High	Medium	Not supporting	High
Methods based on the Kalman filter (KF) [39–41]	Relatively high	Medium	Supporting	Low
Methods based on the least square filters [37,38]	Medium	Low	Supporting	Low
Machine learning based methods [39,40]	High	Medium	Supporting	Low
Simplified electrochemical models [41,42]	High	Very High	Supporting	High
Proposed magnetic field imaging method	High	Medium	Supporting	Low

consuming, and cannot be integrated on-board with the battery management system. To circumvent the limitations of EIS-based methods for SoH estimation, time domain methods are usually recommended such as Ohmic resistance [35] and OCV [36].

A number of HIs have been proposed without the use of electrochemical mechanisms such as the sample entropy of dynamic voltage responses [37]. However, these HIs require consistent discharging profiles, and further validation on unpredictable discharging profiles is still an open question [38].

Adaptive filtering is another SoH estimation approach, which requires a semi-accurate battery model. Several adaptive methods have been used to identify different parameters of LIBs, including the internal resistance for SoH tracking. Kalman filter-based methods (Kalman filter (KF), extended Kalman filter (EKF), Unscented Kalman filter (UKF), Dual EKF, etc.) have been successfully used to estimate battery SoH using different HIs [39–41]. Other widely used algorithms in adaptive filtering are the least square-based ones, specially the recursive least square (RLS) method because of its simple implementation and accuracy [42]. This method gives an accurate estimation of the parameters, directly linked to battery SoH [43].

Electrochemical Models (EM) are complex models that tend to represent the battery behaviour accurately [44]. They are often based on non-linear differential equations. Yet those models can be simplified and combined with adaptive filtering for SoH estimation. In [45], the author simplifies a battery EM before identifying two battery SoH indicators, the internal resistance and the diffusion time, using online recursive parameter identification. To reduce the generated heat, the cell tab arrangements were optimized in [46] using COMSOL electrochemical-electrical thermal modelling. Above studies highlighted the importance of temperature on battery management and tried to control the temperature to ensure safe and reliable operation of batteries. Machine learning methods have also been introduced as an improved model-based technique which simplifies the mathematical framework because of the inherent learning mechanism. Acceptable SoH estimation performance has been reported in [47,48]. These techniques, however, suffer from the need for high volume of training data.

The proposed method in this paper is compared with the reviewed works in Table 1 from the following aspects: accuracy, computational complexity, on-board operation, and time consumption. The proposed SoH estimation process consists of two main components: (1) magnetic field imaging technique and (2) image processing algorithm. This articler only analyses the magnetic field imaging technique to show its feasibility for being an accurate HI source, which can be furthered analysed with different estimation algorithms such as Kalman filters and machine learning estimators.

Adding an online SoH estimator into the BMS of the EVs entails the following added value use cases and applications:

- Vehicle to Grid (V2G) applications can benefit from an online SoH. It helps the microgrid or smart grid management system to optimally prioritise charging/discharging of EVs with different energy costs based on the SoH of the batteries.
- Automatic vehicle maintenance systems can be designed for predictive replacement of aged batteries in order ensure optimal operation of EVs and reduce energy loss due to the ageing issues related with the batteries.
- EV charging stations can better optimise the charging current of the chargers, if the health of the battery is considered. This can increase the lifetime of the battery by choosing the right charging current threshold according to the battery age.

3 | PRELIMINARIES OF CURRENT DENSITY ESTIMATION

Choosing the right method for modelling the charge transport through the electrolyte is the starting point when simulating an electrochemical model since this will determine what physics environment needed for the simulation tools such as COMSOL. In order to apply the correct method of modelling in COMSOL, the user manual of this software has been studied [49].

The electric displacement field in a medium is related to the local charge density according to Gauss's law, one of the Maxwell's equations:

$$\nabla \cdot \mathbf{D} = \rho_v \tag{1}$$

Normally, in electrolyte, it can be assumed that the electrical permittivity is constant and is equal to a bulk value:

$$\mathbf{D} = \varepsilon_0 \varepsilon_s \mathbf{E} = -\varepsilon_0 \varepsilon_s \nabla V \tag{2}$$

Hence

$$\nabla^2 V + \frac{\rho_v}{\varepsilon_0 \varepsilon_s} = 0 \tag{3}$$

In an electrolyte with ionic charge carriers, the charge density can be written as:

$$\rho_v = F \sum_i z_i c_i \tag{4}$$

$$\nabla^2 V + \frac{F}{\varepsilon_0 \varepsilon_s} \sum_i z_i c_i = 0 \tag{5}$$

This is called the Poisson equation that shows the relation between electrolyte potential and the distribution of charge carriers within the electrolyte. It is assumed that ions are the only charge carriers, and the solvated ions and the electric fields don't alter the permittivity of the medium.

The mass transport of the charge carriers in aqueous systems is normally given by the Nernst–Planck equations. These equations neglect ion–ion interactions, and so they are only precise for infinitely dilute solutions:

$$\mathbf{N}_i = -D_i \nabla c_i - z_i u_{m,i} F c_i \nabla \phi_l + c_i \mathbf{u} \tag{6}$$

Concentrated electrolyte is used in many batteries, and to model the mass transport of the charge carriers in this type of systems, usually an extended concentrated species flux definition based on the Maxwell-Stefan set of equations is needed. This will result in a different set of equations to solve for, but the general principles and conclusion in this section will be the same. Therefore, in this case study, the Nernst–Planck equations is used for the calculations.

By substituting the Nernst–Einstein equation for the electrical mobility of an ion we get:

$$\mathbf{N}_i = -D_i \left(\nabla c_i + \frac{z_i F}{RT} c_i \nabla \phi_l \right) + c_i \mathbf{u} \tag{7}$$

The above expressions for the n species i, together with the Poisson equation, give a set of $n + 1$ equations in $n + 1$ unknowns. These are the Nernst–Planck–Poisson equations.

The general mass balance for the diluted species in an electrolyte is described by the following equations for each species i:

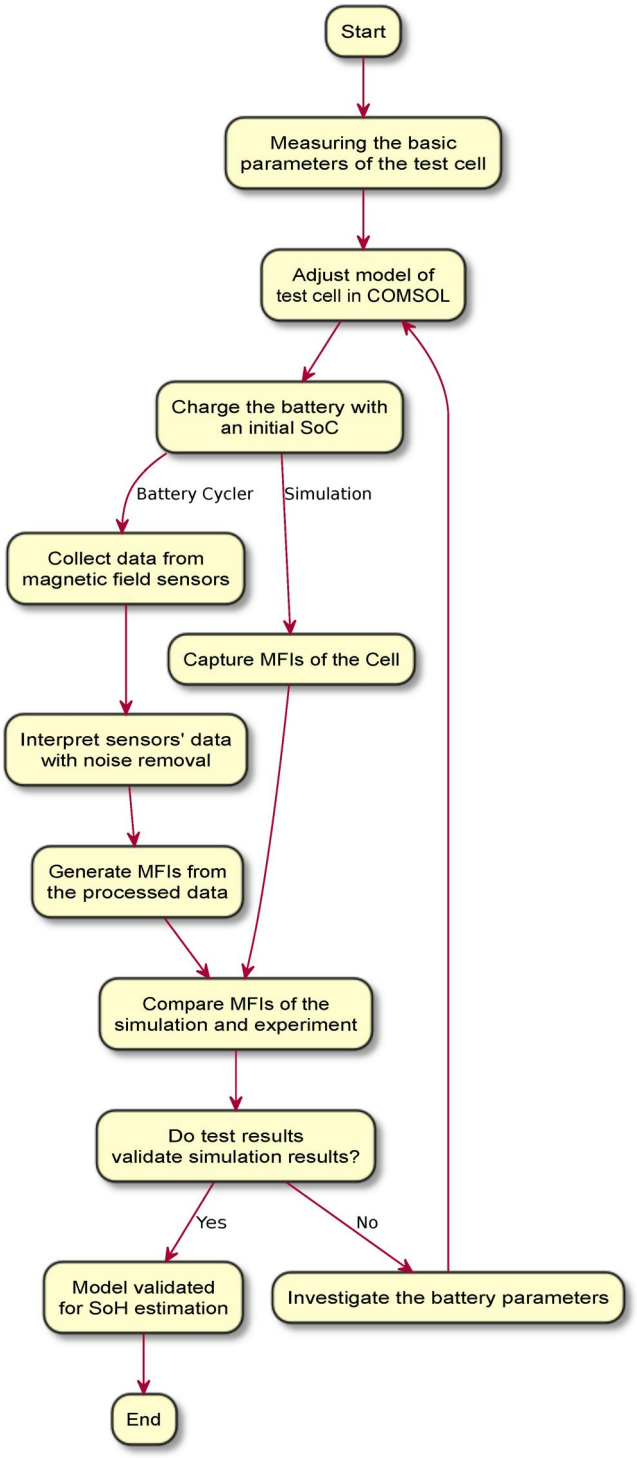

FIGURE 1 Flowchart of the proposed magnetic field imaging method. This flowchart can be used as the reference for application of the SoH estimators in battery management systems of EVs

$$\frac{\partial c_i}{\partial t} + \nabla \cdot \mathbf{N}_i = R_{i,\,\mathrm{tot}} \tag{8}$$

where N_i is the total flux of species i (SI unit: mol/(m^2 · s)). The flux in an electrolyte is described by the Nernst–Planck equations and accounts for the flux of charged solute species

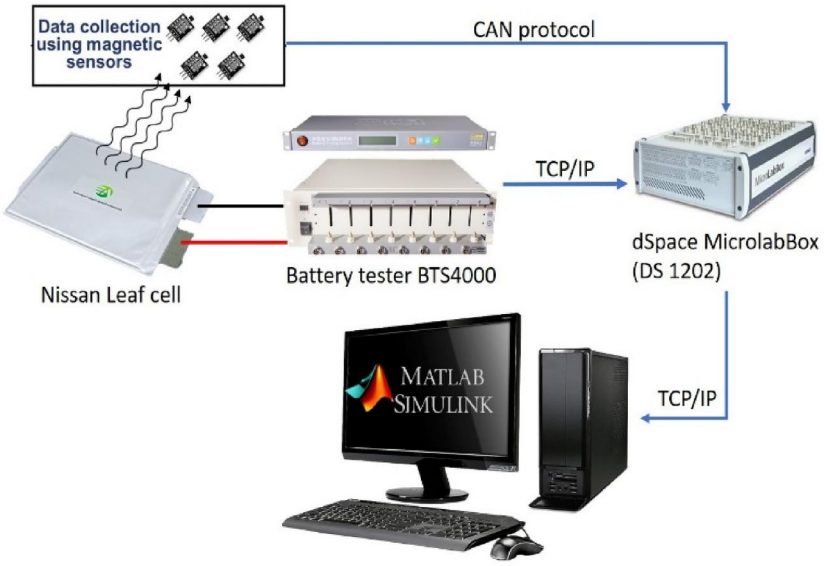

FIGURE 2 Flow diagram of magnetic field imaging process presented in this paper. The equipment includes a battery tester and a real-time simulator, which are connected to the cell and sensors via TCP/IP and CAN protocol. The magnetic field data is collected by the sensors installed on the cell and final results are developed in MATLAB/Simulink

(ions) by diffusion, migration, and convection; these are respectively the first, second, and third term on right side in the equation below.

$$\mathbf{N}_i = -D_i \nabla c_i - z_i u_{m,i} F c_i \nabla \phi_l + c_i \mathbf{u} = \mathbf{J}_i + c_i \mathbf{u} \quad (9)$$

where $\cdot\, c_i$ represents the concentration of the ion i (SI unit: mol/m^3), $\cdot\, z_i$ its valence, $\cdot\, D_i$ the diffusion coefficient (SI unit: m^2/s), $\cdot u_{m,i}$ its mobility (SI unit: $s \cdot mol/kg$), $\cdot F$ denotes the Faraday constant (SI unit: C/mol), $\cdot \phi_i$ the electrolyte potential, $\cdot \mathbf{u}$ is the velocity vector (SI unit: m/s), and $\cdot \mathbf{J}_i$ denotes the molar flux relative to the convective transport.

$$\mathbf{J}_i = -D_i \nabla c_i - z_i u_{m,i} F c_i \nabla \phi_l \quad (10)$$

The net current density can be described using the sum of all species fluxes:

$$\mathbf{i}_l = F \sum z_i \mathbf{N}_i \quad (11)$$

where $\mathbf{i}_l$ denotes the current density vector (SI unit: A/m^2) in the electrolyte. Assuming an electro-neutral situation (which eliminates the convection term) and insignificant concentration gradients of the current-carrying ion (which eliminates the diffusion term), the current density vector in an electrolyte can be written as follows:

$$\mathbf{i}_l = -F^2 \sum z_i^2 u_{m,i} c_i \nabla \phi_l \quad (12)$$

Moreover, by assuming approximately constant composition of charge carriers, a constant electrolyte conductivity is expressed as follows:

$$\sigma_l = F^2 \sum z_i^2 u_{m,i} c_i \quad (13)$$

Therefore, the current density in the electrolyte can be written as:

$$\mathbf{i}_l = -\sigma_l \nabla \phi_l \quad (14)$$

This equation takes the same form as Ohm's law. Therefore, it can be concluded that the charge transport in an electrolyte is ohmic.

Similarly, in an electrode, the electron conduction is modelled using Ohm's law. The domain equation is as follows:

$$\nabla \cdot \mathbf{i}_s = 0 \quad (15)$$

where $\mathbf{i}_s$ shows the current density vector according to:

$$\mathbf{i}_s = -\sigma_s \nabla \phi_s \quad (16)$$

where σ_s shows the electrical conductivity and ϕ_s is the potential of the electron conducting phase.

4 | CURRENT DENSITY ESTIMATION BASED ON MAGNETIC FIELD IMAGING

The theoretical background for calculation of the current density in the electrode and electrolyte was provided in the previous section. In this section, the experimental process for current density measurement based on magnetic fields is provided.

The magnetic field images (MFIs) are captured directly by attaching an array of multiple magnetic sensors on the lithium-ion cell. In Figure 1 the flow chart of the magnetic field imaging process is illustrated. The case study lithium-ion cell is from Nissan Leaf EV battery cell (Figure 2).

As shown in the flowchart of Figure 1, first the model of the cell needs to be initialized with the parameters of the cell under test. Then, raw data from magnetic field sensors are

TABLE 2 Physical parameters of the Nissan leaf cell

Name	Expression	Description
L_sep	30 [um]	Separator thickness
L_pos	60 [um]	Positive electrode thickness
L_neg	60 [um]	Negative electrode thickness
L_pos_cc	10 [um]	Positive current collector thickness
L_neg_cc	10 [um]	Negative current collector thickness
W_cell	216 [mm]	Cell width
H_cell	290 [mm]	Cell height
H_tab	1 [cm]	Tab height
W_tab	14 [cm]	Tab width
L_cell	L_sep + L_pos + L_neg + L_neg_cc/2+L_pos_cc/2	Cell thickness

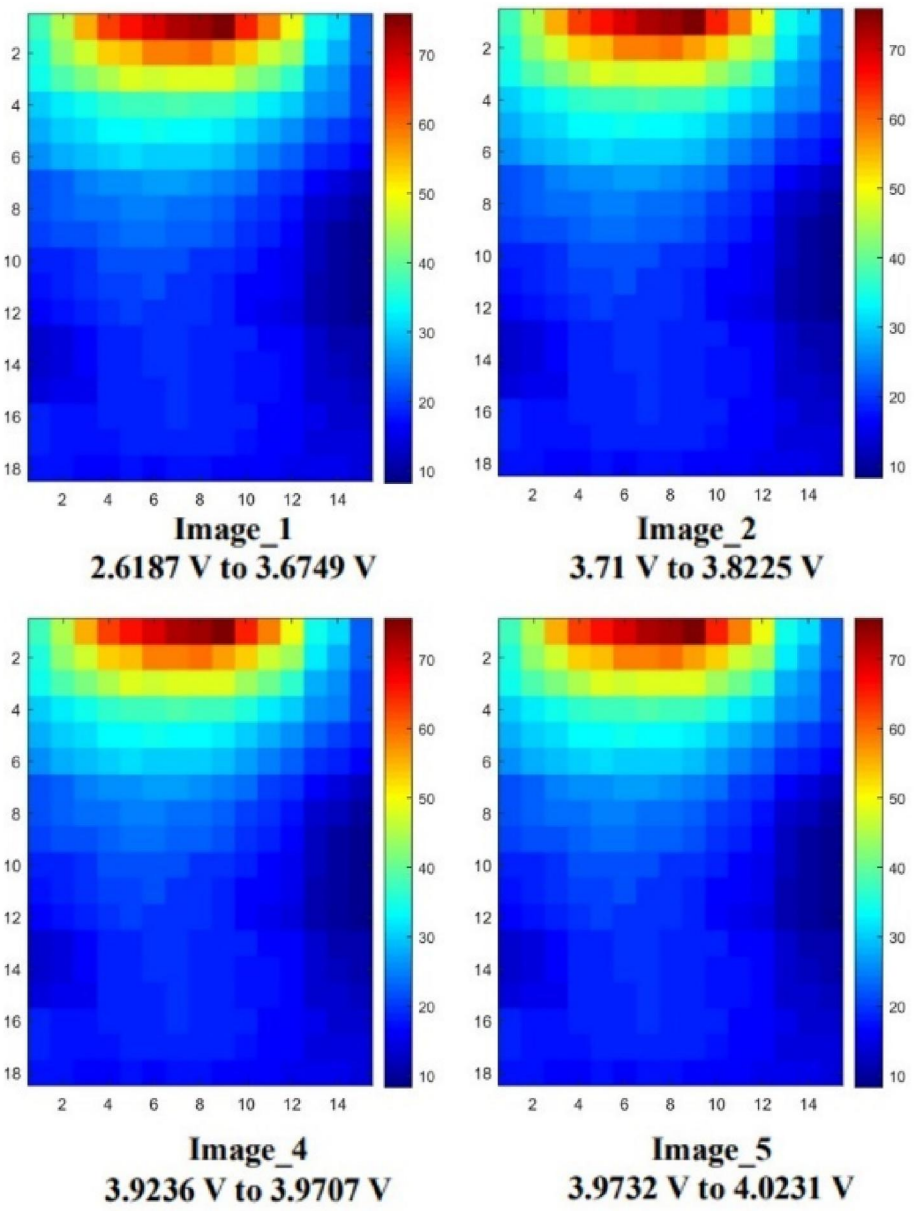

FIGURE 3 Experimental results: magnetic field images captured from the top of the cell in different states of charge during the 10 A charging. Units are in Tesla (T) and tabs are placed on top of the image. It shows negligible changes of magnetic field inside of the current collector

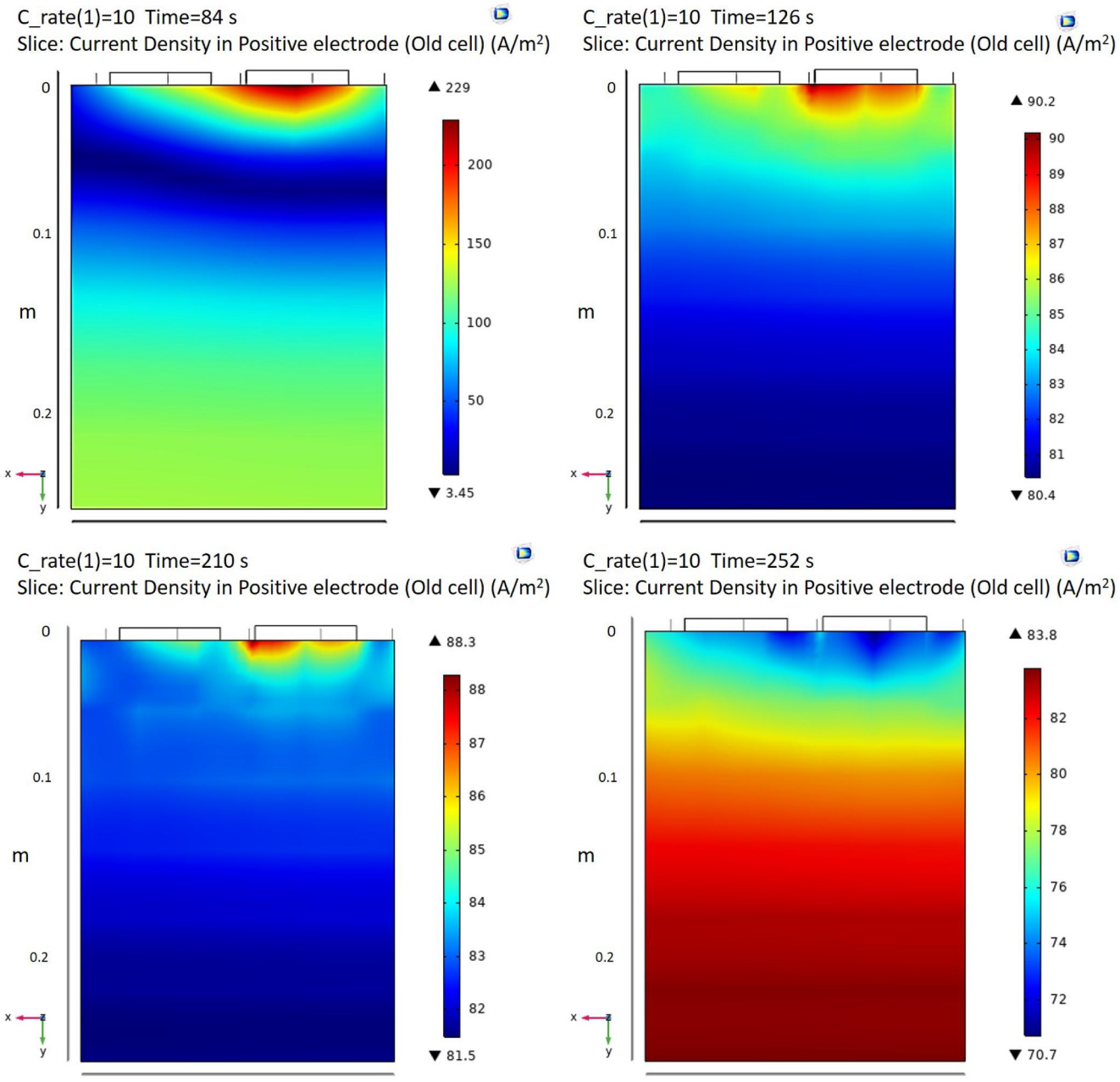

FIGURE 4 COMSOL simulation results: CDIs generated in the positive electrode of the cell at different states of charge during the 10A charging. Unlike what happened in current collectors, it is shown that the current density distribution pattern changes significantly in the positive electrode. Units are in A/m^2

captured and will be processed to generate the MFIs. In this stage, the noise on the data needs to be removed in order to have a clear image of magnetic field. The current density vectors are then calculated directly from the MFIs. The comparison of the MFIs from the magnetic sensors on the test cell and the simulation results of the cell in COMSOL, validates the effectiveness the MFIs for current density computation inside the cells and confirms that it can be used as a health indicator source for the EV batteries.

The eight-channel battery cycler (BTS-4000) is used along with its control unit to emulate different behavioural scenarios on the cell. Each channel is able to provide up to 20 A. In this work, they are used to generate different charging/discharging load cycles for the cell. The battery tester is connected to the Microlabbox via TCP/IP connection. In order to record the load current and output voltage waveform of the cell dSPACE Microlabbox (DS-1202) is used, which provided real-time signals for further data fusion tasks.

Microlabbox was also used for real-time magnetic field data collection from the magnetic sensors installed on the surface of the cell. The recorded data is then processed in MATLAB/Simulink estimation model for online parameter estimation of the equivalent battery model. The quantum fluxgate magnetometers work based on hall effect phenomena. Each

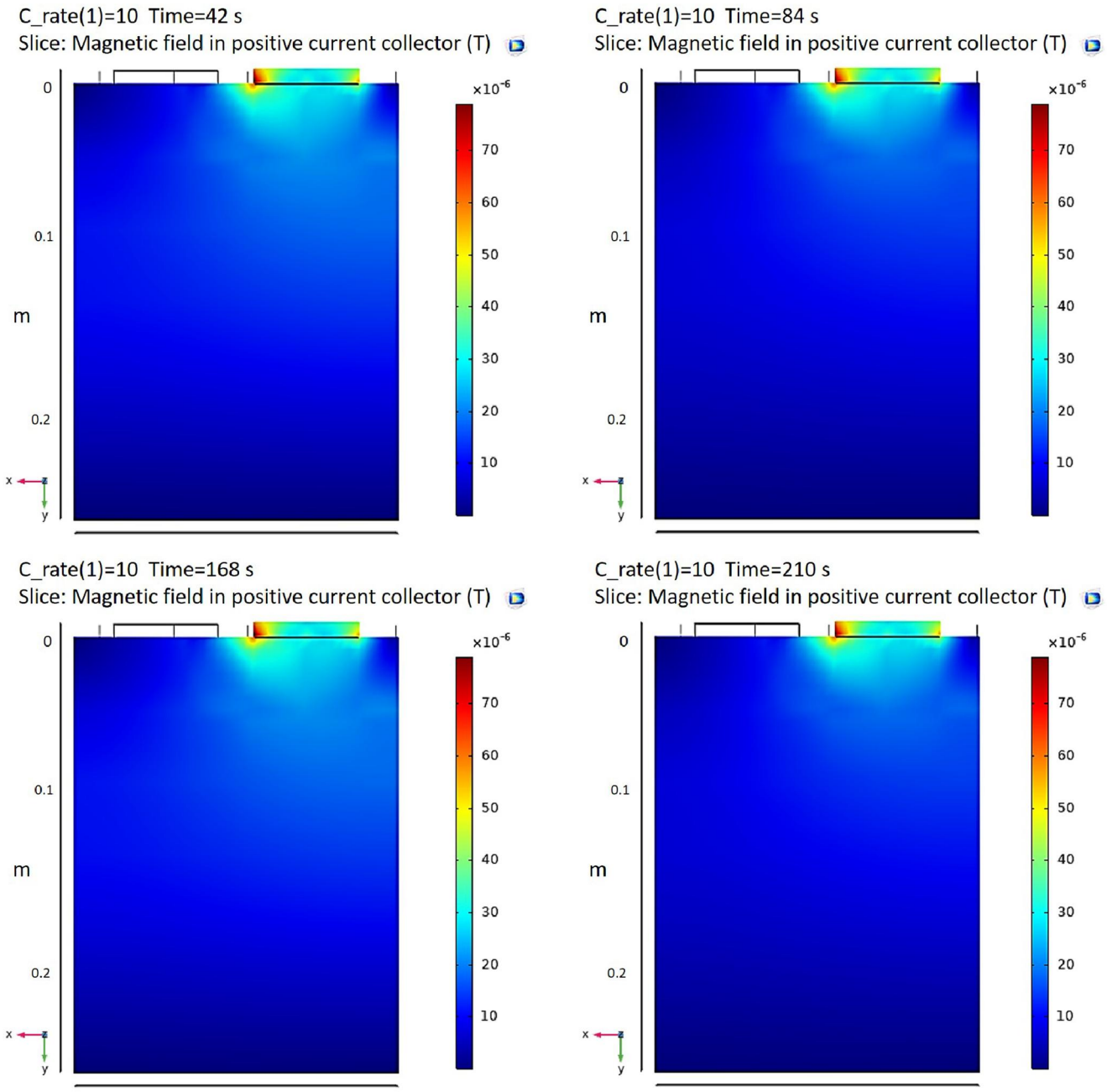

FIGURE 5 Simulation results: magnetic field images generated from the top of the cell in different states of charge during the 10 A charging. Units are in Tesla (T) and tabs are placed on top of the image. The simulated cell was studied at the same point where the sensors were placed, and it is shown that similar results with the actual experiment are repeated

sensor can measure the magnetic field intensity with minimum resolution of ±2 mT. MFIs were taken during different conditions under charge cycles of the battery so there would be a reliable reference available for each state in the cell.

Considering the minimum required accuracy of ±2 mT for magnetic field monitoring in this study, options include using advanced Quantum magnetometers, Hall sensors based on Graphene and Tunnelling Magneto Resistance (TMR) sensors. Being the most economical choice, TMR sensors are used to capture the magnetic field within the cell. On the other hand, owing to the gradual decrease in the price, Hall effect sensors and Quantum magnetometers are the next suitable candidates for magnetic field monitoring.

5 | EXPERIMENTAL RESULTS AND DISCUSSION

As mentioned before, creating an accurate electrochemical model of the cell is necessary for studying the performance of the battery. This method is also used for comparing the expected and the actual results in the case study. In order to

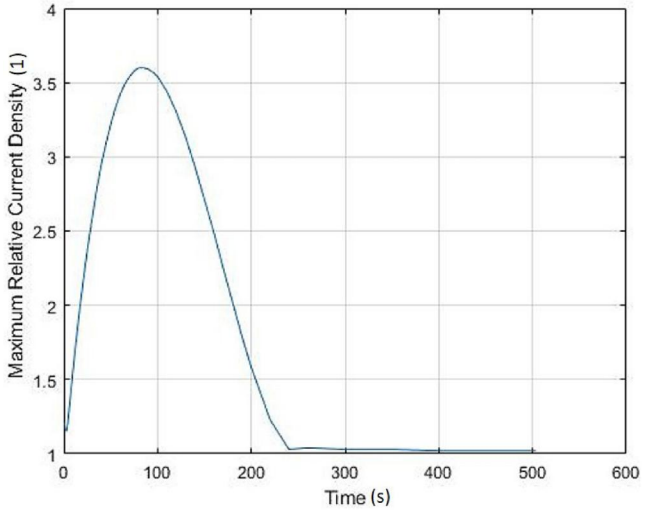

FIGURE 6 Maximum relative current density across the positive electrode during the 10 A charging. This graph shows how the current density magnitude in the positive electrode reaches to a peak during the charging. The vertical axis shows the relative current density, which is $(A/m^2)/(A/m^2) = 1$, and the horizontal axis shows time in seconds

validate the achieved experimental results from the Nissan Leaf battery, a complete and accurate electrochemical simulation of the cell is developed using COMSOL Multi-physics software.

The magnetic field images are captured only during the charging stage of the battery because the discharging current is directly affected by the vehicle operation (driver and control systems). Furthermore, when the EVs are getting charged at the charging station, the car control system is in the park mode that results in having mainly the contribution of battery internal dynamics in the magnetic field images. In order to prepare the cell for next charging cycle, it has been discharged with a constant current of 20 A using the cycler.

The main limitation of the proposed method is the challenge in practical installation of the magnetic field sensors on the cells. EV battery pouch cells are usually compact and because of the space limitation, there is not enough gap to instal the magnetic field sensors. Therefore, in the laboratory experiment, it was necessary to take out the cells and analyse them separately. However, this process can be eased if the sensors get installed in the manufacturing phase of the cells. From the computational point of view, after the model is tuned in the simulation and its results are validated through the capture magnetic field images, it is not necessary to run the computationally expensive processes again. The same models and the results of it can be easily fed into the commonly used image processing algorithms for SoH estimation and ageing prediction.

COMSOL considers a vast set of parameters and has a complete library for each element used to manufacture the cell. During the simulation, the value for most of the parameter used in the model was available in the software's libraries. The physical parameters of the battery, as well as the materials of the electrodes and the electrolyte inside of the cell, are assigned to the domains of the simulated model. Table 2 shows the physical parameters and dimensions of the simulated cell. The parameters related to the materials used in the cell are derived from [16]. A thorough research has been done to find the most accurate values for particle radius, porosity and maximum host capacity for both positive and negative electrodes, to achieve the possible real results [14,15,50].

5.1 | Magnetic field images on top of the positive electrode of an old cell during 10 A charging

The NMC/Graphite cell model simulated in COMSOL has the same size and parameters comparing to the one we used for practical experiments. The aged Nissan Leaf cell we used for testing has a capacity of 27 Ah and the charging process occurred in room temperature, which was 25°C. Unlike the charging behaviour, which usually always follows a specific process, the discharging behaviour in a cell depends on how the battery is being used in the EVs. Therefore, the main goal of this study was to monitor the MFIs generated in the cell and to basically validate the simulation results according to a specific process in the experiments, MFIs were only studied during the charging process with charging currents of 5-A and 10-A. At this stage of work, monitoring MFIs during charging gave us sufficient insight into the changes of SoH in the cell. While charging the existing old Nissan Leaf cell with a charging current of 10A, the magnetic sensors were placed on the cell to capture the value of the magnetic field across the current collector of the cell. In Figure 3, MFIs captured in different states of charge of the cell during the 10A charging are illustrated. It is shown that the magnetic field intensity around the positive tab, where the input voltage is applied, is higher than the rest of the cell.

Simulations in COMSOL validated these results. The MFIs generated in different states of charge of the cell during the 10 A charging of the simulated model is illustrated in Figure 4. According to the Maxwell's original circuital law, magnetic field is directly proportional to the current density. Therefore, it is understood that the current density images (CDIs) across the cell will have the same pattern comparing to the MFIs. The experimental results are successfully validated by the simulation model in COMSOL.

5.2 | Proposed methodology to improve current density monitoring

According to the final MFIs in different states of charge, illustrated in Figure 4, it was observed that almost the same pattern and numbers for each colour-band is repeated as the battery went from fully discharged to fully charged and no noticeable changes happened in the magnetic field captured by the sensors placed on the top of the positive current collector of the cell.

This result seems to be natural as the current collector is made of Aluminium and it somehow acts like a Faraday cage

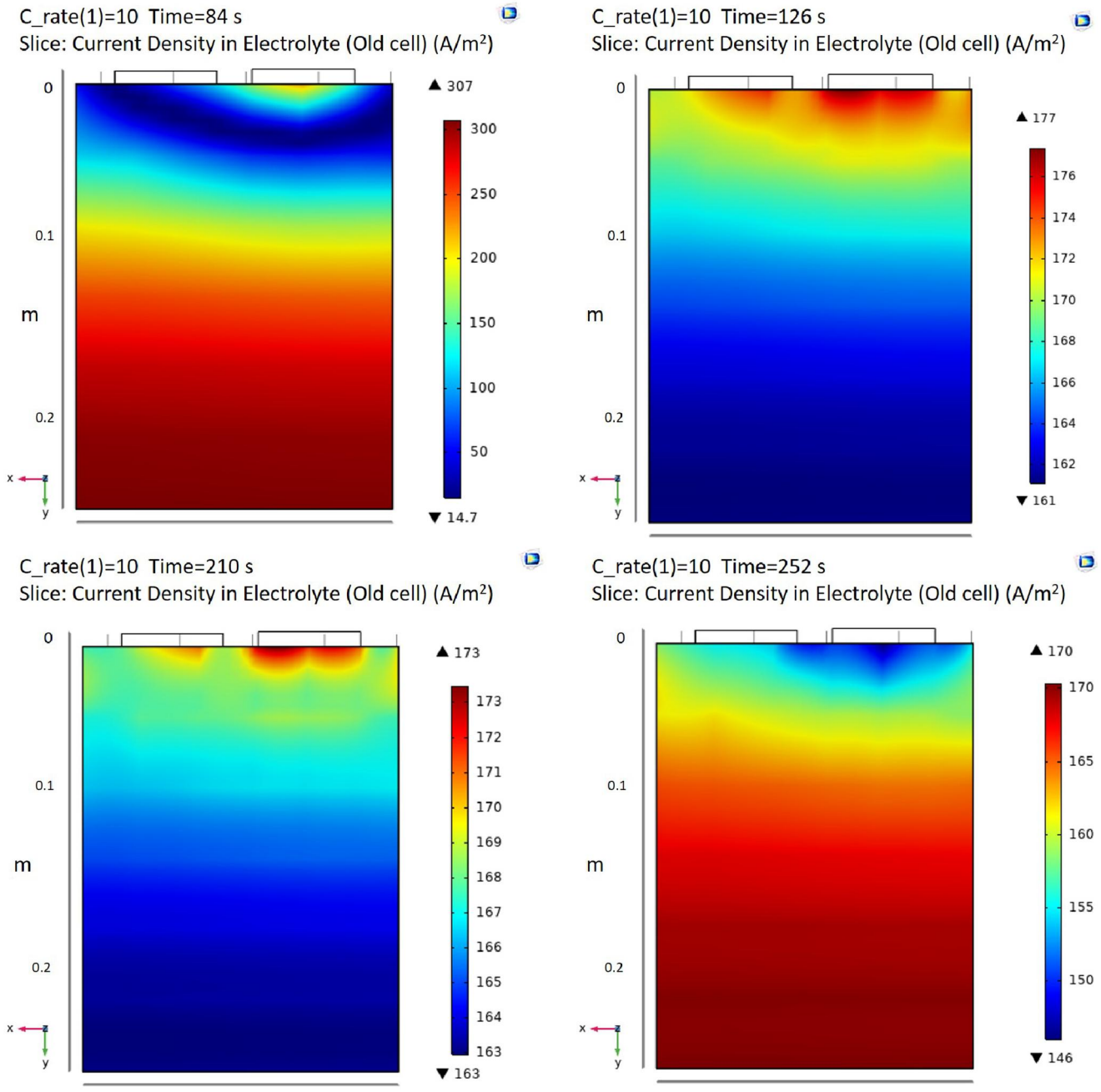

FIGURE 7 COMSOL simulation results: current density images generated in the middle of the electrolyte of the cell at different states of charge during the 10A charging. Units are in A/m^2

and blocks large amount of electromagnetic wave produced inside of the cell. Therefore, it can be concluded that the current methodology to monitor the magnetic field generated by the battery in its different states needs to be improved by implanting the magnetic field sensor in the structure of the lithium-ion cell.

By studying the simulated model in COMSOL, it was understood that the current density distribution and the intensity will change in the cell in different states of charge, but this variation is happening in between of the current collectors, inside of both positive and negative electrodes and also in the electrolyte of the cell. Figure 5 shows the simulation results of CDIs change in the positive electrode of the cell, just under the positive current collector, during the 10 A charging.

It is observed that the current density distribution pattern changes gradually in the positive electrode. During the charging process, the current density across the cell will be uniformed for a short period of time and then, the intensity around the tabs reaches the lowest level compared to the rest of the cell. This pattern of distribution of the current density remains fixed until the cell is nearly charged, although the values assigned to the current density magnitude gradually

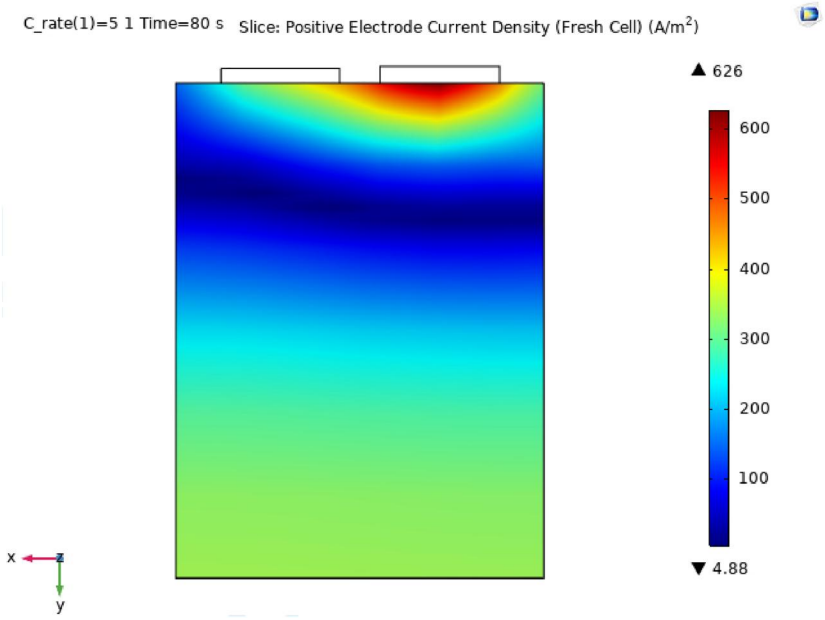

FIGURE 8 Current density images generated in the simulated model of a fresh cell in the middle of 5 A charging duration. The highest current density magnitude is detected around the positive tab. Units are in A/m^2

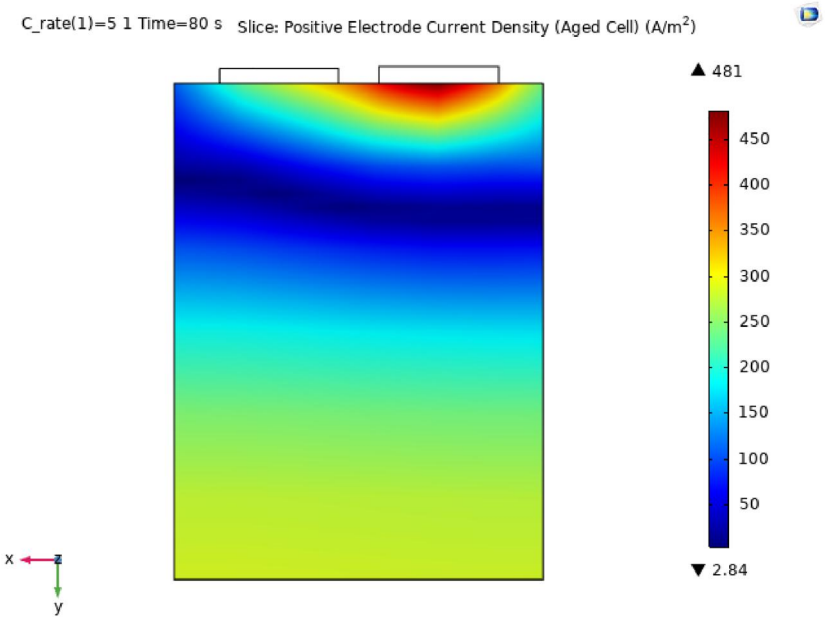

FIGURE 9 Current density images generated in the simulated model of a relatively aged cell in the middle of 5 A charging duration. Similar to a fresh cell, the highest current density magnitude is detected around the positive tab but with a lower value comparing to the fresh cell. Units are in A/m^2

increases to reach a peak. To better show this explanation, the maximum relative current density graph is illustrated in Figure 6. By dividing the cell's 1-C current by the cell's area, a constant value in the form of current density is obtained and relative current density in the cell is then derived by dividing the electrode current density magnitude by this constant value.

CDIs are also changed inside of the electrolyte of the cell during the charging process. Figure 7 shows the simulation results of CDIs variation in the middle of the electrolyte of the cell during the 10A charging.

It can be concluded that by monitoring the magnetic field and subsequently and the the current density inside the positive electrode or the electrolyte, it will be possible to find a meaningful relationship between the captured images and the SoH of the cell. Current density distribution inside the electrolyte follows a similar pattern comparing to the images taken from the positive electrode, therefore, by inserting the magnetic sensors under the aluminium current collector, it would be possible to record the actual internal behaviour of the cell.

5.3 | CDIs derived from simulated model of the cell, in different circumstances

The most important feature, which indicates the SoH in a battery, is the maximum available capacity of the cell. The

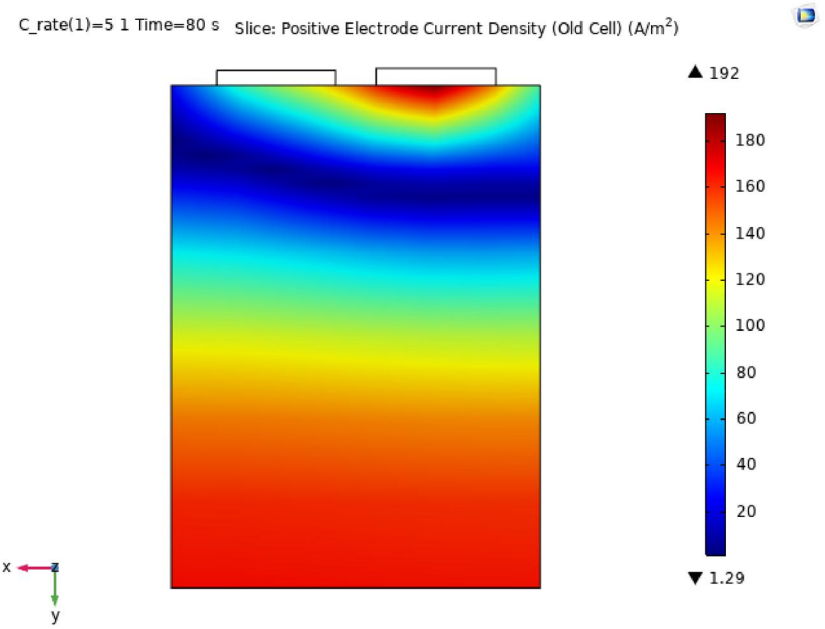

FIGURE 10 Current density images generated in the simulated model of an old cell in the middle of 5 A charging duration. The highest current density magnitude is detected both around the positive tab and at the rear points of the cell. It is also shown that the current density magnitude in an old cell can never be as high as in a fresh cell. Units are in A/m^2

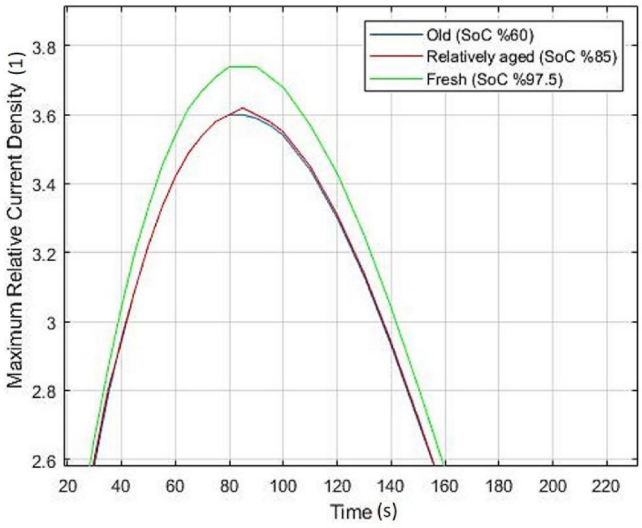

FIGURE 11 Maximum relative current density in a fresh cell, a slightly aged cell and an old cell. As it is indicated, the current density magnitude in a fresh cell reaches its highest possible peak and ageing decreases this peak to some lower values. The vertical axis shows the relative current density, which is $(A/m^2)/(A/m^2) = 1$, and the horizontal axis shows time in seconds

capacity of the simulated cell depends on the physical and chemical parameters of the battery, as well as on the maximum and minimum SoC difference in the cell. The SoC is a parameter with no units and it is usually defined in percentage. The simulated battery is studied during the constant current 5-A charge situation under three different conditions:

1. for a brand-new or a fresh cell: with a maximum full-charge capacity of 97.5%
2. for a relatively aged cell: with a maximum full-charge capacity of 85%
3. for an old cell: with a maximum full-charge capacity of 60%

It was observed that the current density reached a maximum peak in the middle of the charging mechanism and on that point, the difference between the maximum and the minimum level of the current density was maximized. Figures 8–10 show the peak of the current density across the positive electrode in the cell.

It is observed that there is a negligible difference between the two CDIs shown in Figures 9 and 10, as the minimum value of current density distributed at the endpoints of the fresh cell, is slightly greater than in an aged cell and obviously, it is much greater than in an old cell. These images then can be further studied by image processing techniques for better SoH estimation. Moreover, the difference between the maximum and minimum level of current density in a fresh cell, a slightly aged cell and an old cell are 621.12, 478.16, and 190.71 A/m^2, respectively, as displayed on the colour band.

A comparison is also made in Figure 11 in the form of relative current density to show the differences in each type of cell. It can be concluded that as the cell ages, the magnetic field intensity or the current density distribution across the cell becomes more uniform.

6 | CONCLUSION

This article provided an analysis of the current density in electrode and electrolyte of a lithium-ion cell using a simulation assisted method. Early achieved results show that the new proposed method of online current density monitoring in lithium-ion batteries has the potential to improve the state estimation system in a cell. By comparing the practical results and simulation results created in the COMSOL software, it is derived that the simulated electrochemical model of the

lithium-ion cell can be successfully used for further simulation assisted magnetic field and SoH monitoring studies. In future, the information derived from CDIs will be used for predicting the state of certain parameters of the cell using advanced machine learning models in order to build battery management systems with internal ageing estimation functionality.

ORCID

Mehrnaz Javadipour https://orcid.org/0000-0001-8590-476X

REFERENCES

1. Alavi, S.A., et al.: A distributed event-triggered control strategy for dc microgrids based on publish-subscribe model over industrial wireless sensor networks. IEEE Trans. Smart Grid. 10(4), 4323–4337 (2019)
2. Alavi, S. A., Javadipour, M., Mehran, K.: Microgrid Optimal State Estimation Over IoT Wireless Sensor Networks With Event-Based Measurements. . In: IECON 2019 – 45th Annual Conference on IEEE Industrial Electronics Society, Lisbon, Portugal, 2019. pp. 4145–4150. https://doi.org/10.1109/IECON.2019.8927727
3. How, D.N.T, Hannan, M. A., Hossain Lipu, M.S.:Ker, P.J.: State of Charge Estimation for Lithium-Ion Batteries Using Model–Based and Data-Driven Methods: A Review. In: IEEE Access, vol. 7, pp. 136116–136136 (2019). https://doi.org/10.1109/ACCESS.2019.2942213
4. Montazeri, M., Alavi, A., Rahmat jou, H., Ardestani, J. M., & Jadali pour, H.: Real time substation distributed control system simulator development based on IEC 61850 standard for a sample substation (case study: Sheikh Bahayi substation 400/230/63KV), 2013 Smart Grid Conference (SGC), Tehran, Iran, pp. 108–112. (2013). https://doi.org/10.1109/SGC.2013.6733820
5. Amir Alavi, S., Rahimian, A., Mehran, K.:Mehr Ardestani, J.: An IoT-Based data Collection Platform for Situational Awareness-Centric Microgrids. 2018 IEEE Canadian Conference on Electrical & Computer Engineering (CCECE), Quebec City, QC, pp. 1–4 (2018). https://doi.org/10.1109/CCECE.2018.8447718
6. Omariba, Z.B., Zhang, L., Sun, D.: Review on health management system for lithium-ion batteries of electric vehicles. Electron. 7(5) (2018)
7. Alavi, A., Javadipour, M., Afzalian, A.A.: An optimal event-triggered tracking control for battery-based wireless sensor networks. 2016 Smart Grids Conference (SGC), Kerman, pp. 42–47. (2016). https://doi.org/10.1109/SGC.2016.7882950
8. Popp, H., et al.: State estimation approach of lithium-ion batteries by simplified ultrasonic time-of-flight measurement. IEEE Access. 7, 170 992–171 000 (2019)
9. Kim, T., et al.: An on-board model-based condition monitoring for lithium-ion batteries. IEEE Trans. Ind. Appl. 55(2), 1835–1843 (2019)
10. Hu, X., Zheng, Y., Lin, X.:Xie, Y., et al.: Optimal multistage charging of NCA/graphite lithium-ion batteries based on electro-thermal-aging dynamics. IEEE Trans. Transp. Electrif. 6(2), 427–438 (2020). http://dx.doi.org/10.1109/tte.2020.2977092
11. Gao, Y., et al.: Lithium-ion battery ageing mechanisms and life model under different charging stresses. J. Power Sources. 356, 103–114 (2017)
12. Gao, Y., et al.: Health-aware multiobjective optimal charging strategy with coupled electrochemical-thermal-ageing model for lithium-ion battery. IEEE Trans. Ind. Inform. 16(5), 3417–3429 (2020)
13. El Mejdoubi, A., et al.: Lithium-ion batteries health prognosis considering ageing conditions. IEEE Trans. Power Electron. 34(7), 6834–6844 (2019)
14. Bernard, P., et al.: Role of negative electrode porosity in long-term ageing of NMC/graphite Li-ion batteries. J Electrochem. Soc. 162(13), A7096–A7103 (2015)
15. Tsai, P.C., et al.: Single-particle measurements of electrochemical kinetics in NMC and NCA cathodes for Li-ion batteries. Energy Environ. Sci 11(4), 860–871 (2018)
16. Singh, P., Khare, N., Chaturvedi, P.K.: COMSOL Multiphysics® Modelling for li-ion battery ageing. In: Excerpt from Proceedings of 2014 COMSOL Conference. Bangalore, no. 2013, 2 (2014)
17. Yujie, W., Jiaqiang, T. ,Zhendong, S., Li, W., Ruilong, X., Mince, L., Zonghai, C.: A comprehensive review of battery modeling and state estimation approaches for advanced battery management systems. Renewable and Sustainable Energy Reviews, vol. 131. (2020). https://doi.org/10.1016/j.rser.2020.110015
18. Berecibar, M., et al.: Critical review of state of health estimation methods of Li-ion batteries for real applications. Renew. Sustain. Energy Rev. 56, 572–587 (2016)
19. Xiong, R., et al.: Critical review on the battery state of charge estimation methods for electric vehicles. IEEE Access. 6, 1832–1843 (2017)
20. Pop, V., et al.: Accurate state-of-charge indication for battery-powered applications. Battery Management Systems. Philips Research Book Series, vol. 9. Springer Netherlands, Dordrecht (2008). https://www.springer.com/gp/book/9781402069444
21. Meng, J., Boukhnifer, M., Diallo, D.: On-line model-based short circuit diagnosis of lithium-ion batteries for electric vehicle application. In: IECON Proceedings of Industrial Electron. Conference IEEE Computer Society, 2019, 6022–6027.(2019)
22. Weiss, H., Winkler, T., Ziegerhofer, H.: Large lithium-ion battery-powered electric vehicles—From idea to reality. 2018 ELEKTRO, Mikulov, 2018, pp. 1–5 (2018). https://doi.org/10.1109/ELEKTRO.2018.8398241
23. Awadallah, M.A., Venkatesh, B.: Accuracy improvement of SOC estimation in lithium-ion batteries. J. Energy Storage. 6, 95–104 (2016)
24. Li, W., et al.: Electrochemical model-based state estimation for lithium-ion batteries with adaptive unscented Kalman filter. J. Power Sources. 476, 228534 (2020)
25. Ilott, A.J., et al.: Rechargeable lithium-ion cell state of charge and defect detection by in-situ inside-out magnetic resonance imaging/639/638/11/878/639/638/161/891/639/638/675/123/120/128/140/131 article. Nat. Commun. 9(1), 1–7 (2018)
26. Zou, D., et al.: Temperature estimation of lithium-ion battery based on an improved magnetic nanoparticle thermometer. IEEE Access. 8, 135 491–135 498 (2020)
27. Klink, S., Schuhmann, W., La Mantia, F.: Vertical distribution of overpotentials and irreversible charge losses in lithium ion battery electrodes. Chem. Sus. Chem. 7(8), 2159–2166 (2014)
28. Ng, S.-H., La Mantia, F., Novak, P.: A multiple working electrode for electrochemical cells: a tool for current density distribution studies. Angew. Chemie. 121(3), 536–540 (2009)
29. Zhang, G., et al.: Effects of non-uniform current distribution on energy density of Li-ion cells. J. Electrochem. Soc. 160(11), A2299–A2305 (2013)
30. Zheng, Y., et al.: Investigating the error sources of the online state of charge estimation methods for lithium-ion batteries in electric vehicles, 161–188 (2018)
31. Stiaszny, B., et al.: Electrochemical characterisation and post-mortem analysis of aged $LiMn_2O_4$-NMC/graphite lithium ion batteries part II: calendar aging. J Power Sources. 258, 61–75 (2014)
32. Cui, Y., et al.: State of health diagnosis model for lithium ion batteries based on real-time impedance and open circuit voltage parameters identification method. Energy. 144, 647–656 (2018)
33. Din, E., et al.: A scalable active battery management system with embedded real-time electrochemical impedance spectroscopy. IEEE Trans. Power Electron. 32(7), 5688–5698 (2017)
34. Zhou, X., et al.: An easy-to-implement multi-point impedance technique for monitoring aging of lithium ion batteries. J. Power Sources. 417, 188–192 (2019)
35. Chen, L., et al.: A new state-of-health estimation method for lithium-ion batteries through the intrinsic relationship between ohmic internal resistance and capacity. Meas. J. Int. Meas. Confed. 116, 586–595 (2018)
36. Tian, J., Xiong, R., Yu, Q.: Fractional-order model-based incremental capacity analysis for degradation state recognition of lithium-ion batteries. IEEE Trans. Ind. Electron. 66(2), 1576–1584 (2019)

37. Hu, X., et al.: Battery health prognosis for electric vehicles using sample entropy and sparse Bayesian predictive modeling. IEEE Trans. Ind. Electron. 63(4), 2645–2656 (2016)
38. Tian, J., Xiong, R., Shen, W.: A review on state of health estimation for lithium ion batteries in photovoltaic systems, eTransportation, vol. 2, 100028. (2019). https://doi.org/10.1016/j.etran.2019.100028
39. Omariba, Z.B., et al.: Parameter identification and state estimation of lithium-ion batteries for electric vehicles with vibration and temperature dynamics. World Electr. Veh. J. 11(3), 50 (2020)
40. Shen, P., et al.: The co-estimation of state of charge, state of health, and state of function for lithium-ion batteries in electric vehicles. IEEE Trans. Veh. Technol. 67(1), 92–103 (2018)
41. Zhu, Q., et al.: A state of charge estimation method for lithium-ion batteries based on fractional order adaptive extended Kalman filter. Energy. 187, 115880 (2019)
42. Rozaqi, L., Rijanto, E., Kanarachos, S.: Comparison between RLS-GA and RLS-PSO for Li-ion battery SOC and SOH estimation: a simulation study. J. Mechatronics Electr. Power, Veh. Technol. 8(1), 40 (2017)
43. Rijanto, E., et al.: RLS with optimum multiple adaptive forgetting factors for SoC and SoH estimation of Li-Ion battery. In: Proceedings 2017 5th International Conference Instrumentation, Control. Autom. ICA 2017, Institute of Electrical and Electronics Engineers Inc., 73–77 (2017)
44. Prasad, G.K., Rahn, C.D.: Model based identification of ageing parameters in lithium ion batteries. J. Power Sources. 232, 79–85 (2013)
45. Jaguemont, J., Boulon, L., Dubé, Y.: Characterisation and modeling of a hybrid-electric-vehicle lithium-ion battery pack at low temperatures. IEEE Trans. Veh. Technol. 65(1), 1–14 (2016)
46. Zhang, X., et al.: Electrochemical-electrical-thermal modelling of a pouch-type lithium ion battery: an application to optimise temperature distribution. J. Energy Storage. 11, 249–257 (2017)
47. Pan, H., et al.: Novel battery state-of-health online estimation method using multiple health indicators and an extreme learning machine. Energy. 160, 466–477 (2018)
48. Li, P., et al.: State-of-health estimation and remaining useful life prediction for the lithium-ion battery based on a variant long short term memory neural network. J. Power Sources. 459, 228069 (2020)
49. COMSOL: Electrodeposition Module User's Guide. COMSOL, Inc. 100 District Avenue Burlington, MA 01803 USA (2019). https://doc.comsol.com/5.4/doc/com.comsol.help.edecm/ElectrodepositionModuleUsersGuide.pdf
50. Chen, C.-H., et al.: Development of experimental techniques for parameterisation of multi-scale lithium-ion battery models. J. Electrochem. Soc. 167(8), 080534 (2020)

How to cite this article: Javadipour M, Mehran K. Analysis of current density in the electrode and electrolyte of lithium-ion cells for ageing estimation applications. *IET Smart Grid*. 2021;4:176–189. https://doi.org/10.1049/stg2.12018